Theor. Comput. Fluid Dyn. (2010) 24:483–496
DOI 10.1007/s00162-010-0180-z

ORIGINAL ARTICLE

**Bo Hoffmann Jørgensen · Jens Nørkær Sørensen · Nadine Aubry**

# Control of vortex breakdown in a closed cylinder with a rotating lid

Received: 10 November 2008 / Accepted: 19 November 2009 / Published online: 3 February 2010


**Abstract** The flow within a closed cylinder with a rotating lid is considered as a prototype for fundamental studies of vortex breakdown. Numerical simulations for various parameter values have been carried out to reproduce the known effect of a thin rotating rod positioned along the center axis as well as analyze the influence of local vorticity sources. As expected, the results show that the breakdown bubbles in the steady axisymmetric flow can be affected dramatically, i.e., fully suppressed or significantly enhanced, by rotating the rod. The main contribution of this article is to show that the observed behavior can be explained by the vorticity generated by the rod locally near the rotating lid and near the fixed lid, as analogous behavior is caused by the introduction of local vorticity sources in the flow without a rod. Moreover, we describe the influence on the breakdown bubbles of the vorticity sources by an analytical model. In addition to improving our understanding, this finding should also open the door to other types of flow control devices capable of generating localized vorticity.

**Keywords** Laminar flows in cavities · Vortex breakdown suppression · Flow control · Rotating flow

## 1 Introduction

Vortex breakdown has been the subject of numerous studies as it is crucial to many technical applications. However, it is not fully understood and remains difficult to predict and control. Generic studies of mechanisms capable of controlling vortex breakdown are steps in the direction of understanding and controlling this phenomenon better.

In this article, we concentrate our efforts on vortex breakdown in a confined geometry, specifically a flow in a closed cylinder with a rotating lid. Such an approach offers several advantages compared to an open

**Electronic supplementary material** The online version of this article (doi:10.1007/s00162-010-0180-z) contains supplementary material, which is available to authorized users.

Communicated by H. Aref

B. H. Jørgensen (✉) · J. N. Sørensen
Department of Mechanical Engineering, Fluid Mechanics Section, Technical University of Denmark,
Building 403, 2800 Lyngby, Denmark
E-mail: bo.hoffmann@gmail.com

J. N. Sørensen
E-mail: jns@mek.dtu.dk

N. Aubry
Department of Mechanical Engineering, Carnegie Mellon University, Pittsburgh, PA 15213-3890, USA
E-mail: aubry@andrew.cmu.edu

flow model. First, it is free of external, ambient disturbances that are often present in open flows; second, the boundary conditions of the fluid mechanics problem are well-defined. However, one has to keep in mind the specific conditions under which a closed flow configuration works. Such a flow was originally introduced experimentally by Vogel [29] and Ronnenberg [17], and was further studied by Escudier [6].

Due to the simple geometry of the closed cavity and the existence of efficient axisymmetric Navier–Stokes solvers, this type of problem is highly suitable for numerical studies. While the transition scenario in the flow has been studied numerically by Sørensen and Christensen [20], Gelfgat et al. [7] have investigated the stability of steady states and the evolution of breakdown bubbles. Earlier numerical studies include those of Lugt and Abboud [12], Lopez [11], and Brown and Lopez [2], with the latter authors presenting a criterion for vortex breakdown based on the change of sign in vorticity. A number of studies have also addressed the unsteady flow and three-dimensional effects in the closed cylinder either experimentally [26] or numerically [1,18,23–25].

During the last 15 years or so, there have been many attempts to control fluid flows. One generic flow control technique consists of introducing vorticity sources in the flow. For instance, Tang and Aubry [27] performed a study of the symmetry breaking instability leading to vortex shedding in the flow past a cylinder and investigated the effect of small vorticity perturbations placed along the stable and unstable eigenspaces of the fixed point of a reduced model. Their findings were subsequently used for controlling vortex shedding and its onset in the physical flow [28].

Like in the case of other fluid flows, it became clear that the closed cavity flow with a rotating lid could greatly benefit from control strategies. This flow was indeed controlled by means of a rotating axial rod by Husain et al. [9] who reported flow visualization experiments, while also presenting an analytical model aimed at explaining the observed phenomena. Their analytical model neglected the axial variation of the flow velocity, and, therefore, the presence of various breakdown bubbles along the axis. In a later article, Husain et al. [10] extended their experimental investigation using laser-induced fluorescence (LIF) and presented an alternative analytical model, arguing that the rod co-rotation decreases the unfavorable pressure gradient along the axis, thus suppressing the breakdown bubbles.

Mullin et al. [13] numerically investigated a slightly different configuration in which both end-walls rotate. In order to control such a flow, these authors explored the effect of both a rotating and a stationary inner cylinder. The configuration with the inner cylinder was also considered in Mullin et al. [14], although the rotating lid and the inner cylinder were not independent in their study. Moreover, sloped cylinder walls were used as an alternative control mechanism in the latter article. Other techniques to control vortex breakdown consisted of introducing a cone [16] and suppressing the no-slip conditions on the container walls [19].

The goal of the present numerical study is to control, i.e., either suppress or enhance, the breakdown bubbles of the axisymmetric and steady flow in a closed cylinder with straight walls and a rotating lid, as well as investigate the fundamental fluid mechanics phenomenon enabling the control. For this purpose, we first insert a thin rotating rod along the center axis and determine its effect on the flow. While our findings agree with those experimentally obtained by Husain et al., we also show that similar results can be achieved by fully withdrawing the rod and introducing strategically located vorticity sources. We also discuss the underlying fundamental control mechanism by exploring the role played by these vorticity sources in the vorticity transport equation and derive the additional axial velocity induced by such sources using the Biot–Savart law. This approach allows us to not only understand the role played by the rotating rod in terms of the physics involved but also consider more generalized control techniques, including the suppression of breakdown bubbles through the counter-rotation of a small disk opposite to the driving lid, as observed experimentally by Mununga et al. [15].

In this study, we restrict ourselves to one value of the aspect ratio (ratio between the height and the radius of the cylinder), specifically an aspect ratio of 2.0. The transition to three-dimensional flow for this aspect ratio has been studied numerically by Gelfgat et al. [7] and experimentally by Sørensen et al. [22], who showed that the flow remains axisymmetric in the various steady regimes as well as in a substantial part of the unsteady domain. Since we are concerned here with the various steady flow patterns, it is reasonable to restrict ourselves to axisymmetric calculations.

This article is organized as follows. In Sect. 2, we formulate the problem, and in Sect. 3, we present the governing equations and the numerical method used. We then discuss our numerical results in Sects. 4 and 5, which we complement by theoretical arguments, and draw our conclusions in Sect. 6.

## 2 Problem formulation

We first consider the basic configuration, as shown in Fig. 1, consisting of a closed cylinder with a rotating lid with and without a rotating rod on the cylinder axis. While the main effect of the rotating lid is to set

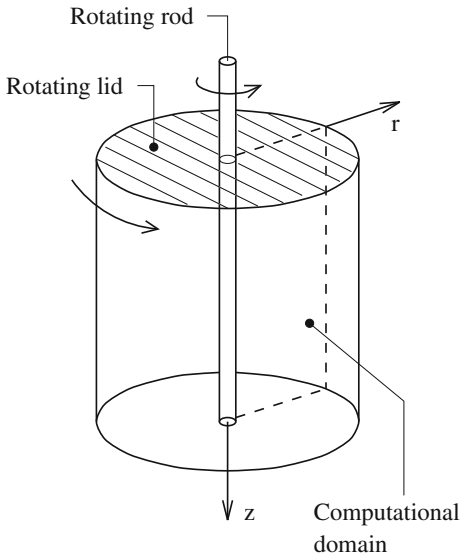


**Fig. 1** Schematics of the flow configuration studied in this article. Cylindrical cavity with rotating lid and rotating rod. The considered domain is a plane in between the rod and the wall

the fluid into a rotating motion around the center axis, it also drives the fluid close to the lid away from the center, thereby causing a meridional circulation. The fluid leaving the area near the lid then travels downwards along the outer wall, turns inwards near the fixed lid, rises vertically close to the center axis and returns to the area near the rotating lid. Along this path, the azimuthal flow velocity component undergoes changes and the fluid rising along the center axis forms a strong swirling vortex core. This vortex may experience vortex breakdown, which manifests itself by one or more bubble-like zones of recirculating fluid, commonly referred to as breakdown bubbles, that are located along the center axis (see Fig. 2).

The dimensionless parameters governing the flow consist of the aspect ratio

$$\lambda = H/R, \tag{1}$$

where $H$ and $R$ denote the height and the radius of the cylinder, respectively, and the Reynolds number

$$Re_{\text{lid}} = \frac{v_{\text{lid}} R}{\nu}, \tag{2}$$

where $v_{\text{lid}}$ refers to the tip velocity of the lid and $\nu$ is the kinematic viscosity of the fluid.

Escudier [6] identified boundaries within the $(\lambda, Re_{\text{lid}})$-parameter plane in which zero, one, two, or three breakdown bubbles occur on the center axis. In addition, for any given aspect ratio, there is a critical Reynolds number, $Re_{\text{c}}(\lambda)$, at which the flow becomes unsteady and begins to oscillate. Escudier found that, for Reynolds numbers slightly larger than $Re_{\text{c}}(\lambda)$, the oscillation is periodic and axial provided that $\lambda < 3.1$. As mentioned earlier, we restrict ourselves to an aspect ratio of $\lambda = 2.0$. For this particular value, the only possible configurations contain zero, one, or two breakdown bubbles. The streamlines of the flow obtained with our numerical simulation are presented in Fig. 2 for the Reynolds number value $Re_{\text{lid}} = 2200$, and are compared with an experimental visualization of the flow. In this case, both the simulation and experimental results exhibit two breakdown bubbles at approximately the same locations, thus showing good qualitative agreement.

As shown in Sørensen and Loc [21], the axisymmetric flow can be accurately described by transport equations for the vorticity and the azimuthal velocity, and a Poisson equation for the streamfunction. This property is used in our numerical approach.

In order to control vortex breakdown, i.e., either suppress or enhance the breakdown bubbles, a thin rod with radius $\delta = 0.02R$ is introduced in the numerical model (see Fig. 1).

A simple dimensional analysis of this alternate problem yields four dimensionless model parameters. These are, besides the aspect ratio $\lambda$, the Reynolds number $Re_{\text{lid}}$, the ratio between the radius of the rod and that of the cylinder,

$$\xi = \delta/R, \tag{3}$$

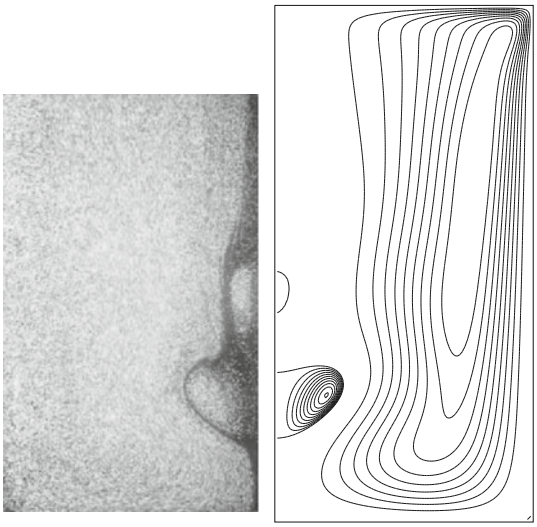

**(a)** **(b)**

**Fig. 2** Comparison between experiment and computed streamlines for $Re_{\text{lid}} = 2200$. **a** Visualization: particles appear as white spots in a laser sheet. **b** Streamlines from numerical simulation

and the ratio between the Reynolds number of the rod and that of the cylinder,

$$\gamma = \frac{v_\delta \delta}{v_{\text{lid}} R} = \frac{Re_\delta}{Re_{\text{lid}}}, \tag{4}$$

where $v_\delta$ is the surface velocity of the rod. $Re_\delta$ is the Reynolds number based on this velocity. In order to further reduce the number of control parameters in our problem, we set $\xi = 0.02$. Since $\lambda = 2.0$, the two remaining parameters which will be varied in this article are the Reynolds number ratio $\gamma$, and the Reynolds number associated with the lid rotation $Re_{\text{lid}}$.

## 3 Governing equations and numerical method

The axisymmetric formulation can be derived in a straightforward manner using the Poisson equation, the azimuthal component of the Navier–Stokes equations in cylindrical coordinates, and the vorticity transport equation in rotational form, as we now recall.

Using the streamfunction $\psi$ such that

$$v_r = \frac{1}{r}\frac{\partial \psi}{\partial z}, \quad v_z = -\frac{1}{r}\frac{\partial \psi}{\partial r} \tag{5}$$

and letting $\omega$ be the azimuthal component of the vorticity, the Poisson equation for the streamfunction takes the expression

$$\frac{\partial^2 \psi}{\partial z^2} + \frac{\partial^2 \psi}{\partial r^2} - \frac{1}{r}\frac{\partial \psi}{\partial r} = r\omega. \tag{6}$$

The azimuthal velocity and vorticity transport equations are given by

$$\frac{\partial v_\theta}{\partial t} = -\frac{\partial}{\partial r}(v_r v_\theta) - \frac{\partial}{\partial z}(v_z v_\theta) - \frac{2}{r} v_r v_\theta + \frac{1}{Re_{\text{lid}}}\left[\frac{\partial}{\partial r}\left(\frac{1}{r}\frac{\partial (r v_\theta)}{\partial r}\right) + \frac{\partial^2 v_\theta}{\partial z^2}\right], \tag{7}$$

$$\frac{\partial \omega}{\partial t} = -\frac{\partial}{\partial r}(v_r \omega) - \frac{\partial}{\partial z}(v_z \omega) + \frac{1}{r}\frac{\partial}{\partial z}(v_\theta^2) + \frac{1}{Re_{\text{lid}}}\left[\frac{\partial}{\partial r}\left(\frac{1}{r}\frac{\partial (r\omega)}{\partial r}\right) + \frac{\partial^2 \omega}{\partial z^2}\right], \tag{8}$$

where the variables have been made dimensionless using $R$ and $v_{\text{lid}}$ as reference length and velocity scales. For a closed cylinder with a rotating lid, we apply the boundary conditions of Sørensen and Loc [21], namely

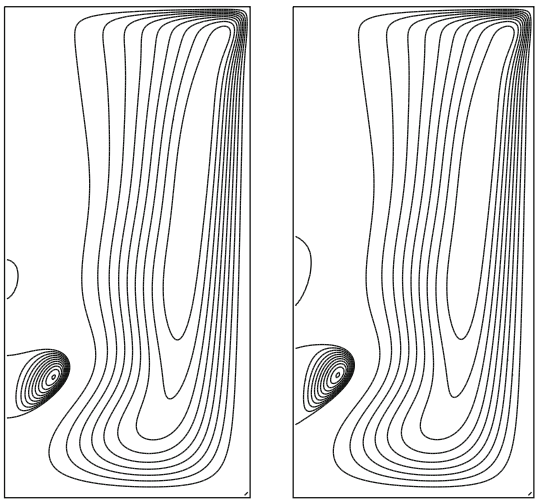

**(a)** **(b)**

**Fig. 3** Effect of introducing a rod at $Re_{\text{lid}} = 2200$. The streamline plots utilize a cubic function of the streamfunction, which makes the breakdown bubbles appear prominently. **a** Original flow, **b** flow with a fixed rod

the symmetry condition with respect to the center axis and the no-slip condition on the cylinder wall, the rotating lid, and the fixed lid. The rotating rod with radius $\delta$, as shown in Fig. 1, was introduced by replacing the symmetry condition with respect to the center axis by the appropriate no-slip condition.

In this article, we use the finite-difference code developed at LIMSI/CNRS in France and based on the former equations (see [4,5,21] for more details). The ability of the numerical procedure to correctly reproduce the flow structures is demonstrated in Fig. 2, where a photograph obtained by Buchhave et al. [3] using particle image velocimetry (PIV) can be compared qualitatively side-by-side with the computed streamlines. There is an optical effect expanding the image of the bubbles in the experiment because large particles do not follow the flow. For a quantitative comparison, we refer the reader to Sørensen and Loc [21], who carefully validated the basic numerical code (without rod) against both visualizations and velocity profiles obtained by Laser Doppler Anemometry (LDA). We thus consider the numerical method thoroughly validated.

By investigating different grid sizes, a grid resolution of $\Delta r = \Delta z = 0.01$ was found to be sufficient within the parameter range of interest in this article. In particular, quantitative resolution plots (not shown here) have been obtained for the flow with a rod. The solution was found to converge with an increasing number of grid cells when the rod keeps its fixed physical size.

## 4 Results

### 4.1 Effect of introducing a fixed rod

In order to analyze the effect of introducing a fixed rod in the flow, we compared streamlines for the case without a rod to those obtained in the presence of a fixed rod. The results are shown in Fig. 3, where it is clear that in both situations the flow exhibits two breakdown bubbles for the Reynolds number $Re_{\text{lid}} = 2200$. Note that the streamline plots were obtained by a cubic function of the streamfunction to ensure a prominent appearance of the breakdown bubbles. It is observed that introducing a fixed rod slightly alters the size of the second bubble, while leaving the basic flow structure unchanged. Although this effect is not dramatic, it is noticeable as the rod does not follow the bulk flow rotation. This has a relatively small influence on the flow (somewhat similar to counter rotation), causing the breakdown bubbles to enlarge slightly.

### 4.2 Effect of introducing a rotating rod

The effect of co-rotation ($\gamma > 0$) and counter-rotation ($\gamma < 0$) of the rod relative to the lid for $Re_{\text{lid}} = 2200$ is displayed in Fig. 4 for various values of the Reynolds number ratio $\gamma$. These results, although known from

experimental investigations, to the best of our knowledge have not been obtained, so far, using numerical simulations. Specifically, it is found that co-rotation causes the smaller breakdown bubble to vanish at a $\gamma$-value within the interval $0.001 < \gamma < 0.002$ and the larger breakdown bubble to disappear at a $\gamma$-value within $0.004 < \gamma < 0.005$. Furthermore, our numerical simulations reveal that the appearance of a small vortex in the upper left-hand corner of the computational domain close to the intersection between the rod and the lid, clearly visible for the $\gamma$ values of $\gamma = 0.004$ and $\gamma = 0.006$, a phenomenon not previously reported. Counter-rotation also creates a vortex in the upper left-hand corner of the computational domain. However, in contrast to co-rotation, counter-rotation causes the size of the two breakdown bubbles to increase. In addition, the flow becomes unsteady at a $\gamma$-value in the range of $-0.007 < \gamma < -0.006$. We, therefore, conclude that both co-rotation and counter-rotation have a dramatic effect on the flow structure near the rod. These findings are consistent with those obtained experimentally by Husain et al. [9] for the parameter values $Re_{\text{lid}} = 2720$, $H/R = 3.25$, and $\xi = 0.0416$, in which the latter authors observed three breakdown bubbles for a fixed rod. With increasing co-rotating angular velocity, the bubbles became progressively smaller in size and finally disappeared, while a slow counter-rotation of the rod led to more prominent and wider bubbles than those observed with the fixed rod. These results also agree with the recent experimental study by Husain et al. [10] as well as with the numerical study by Herrada and Shtern [8] in the case of a near-axis swirl.

In order to gain insight into the mechanisms at play, it is instructive to study the transient between two equilibrium states. One may indeed wonder what happens with the breakdown bubbles in the transient flow as one starts to rotate the rod. In order to address this issue, we performed the three-step simulation illustrated in Fig. 5. First, the steady flow with a fixed rod was calculated for $Re_{\text{lid}} = 2200$. Second, the breakdown bubbles were visualized numerically by injecting tracing particles near the rod close to the fixed lid, with an image of tracing particles appearing in the core of the flow (see Fig. 5). Finally, after suddenly starting a co-rotation of the initially fixed rod at time $t = 0$, the breakdown bubbles moved up and dissipated in the boundary layer of the rotating lid. Then, the flow gradually became steady and the breakdown bubbles did not reappear.

### 4.3 Formation of corner vorticity sources as the rod rotates

It is interesting to note that even though co-rotation causes the breakdown bubbles to disappear, a vortex is formed in the corner between the rotating lid and the rod, as shown in Fig. 4. In this subsection, we show that its presence is key to understanding the underlying physics of the control mechanism. For this, we now turn to the vorticity transport equation (Eq. 8). A careful inspection of this equation shows that the only way the rotational motion introduced by the rod can affect the vorticity, and thus the flow behavior in the meridional plane, is through the source term

$$S = \frac{1}{r}\frac{\partial}{\partial z}\left(v_\theta^2\right). \tag{9}$$

At the surface of the rotating rod, this term is zero as $v_\theta$ is independent of $z$ there. Away from the rod, this term is also expected to not have a significant effect on the flow behavior as the azimuthal velocity introduced by rotating the rod is mainly a function of $r$. In the corner between the lid and the rod, however, the azimuthal velocity $v_\theta$ experiences a jump from the speed of the lid to the speed of the rod. As it is clear from Eq. 9, such an abrupt change necessarily creates a vorticity source term just below the rotating lid. Furthermore, this source term, which takes a positive value in the case, where the surface of the rod moves at a speed higher than that of the lid at the radius $\delta$, generates a velocity field according to the induction law of Biot–Savart (subject to the boundary conditions of a confined domain). The latter induction law creates a domain of influence which is directed downwards along the symmetry axis, so that a positive source term induces an axial velocity against the direction of the bulk flow. Note that this observation is independent of whether the rod is subject to co-rotation or counter-rotation, due to the fact that the source term contains the axial derivative of the square of the azimuthal velocity. Furthermore, the surface of the rod moves at a speed higher than that of the lid at the radius $\delta$ when $\gamma^2 > (\delta/R)^4$ (as seen by inserting $v_\delta = v_{\text{lid}}\delta/R$ into Eq. 4).

Likewise, a similar vorticity source has to appear in the corner between the rotating rod and the fixed lid. Since at the fixed lid $v_\delta^2$ is positive, inserting the appropriate scales into Eq. 9, we obtain

$$S \sim -\frac{R^2 v_{\text{lid}}^2}{\rho\delta^3}\gamma^2,$$

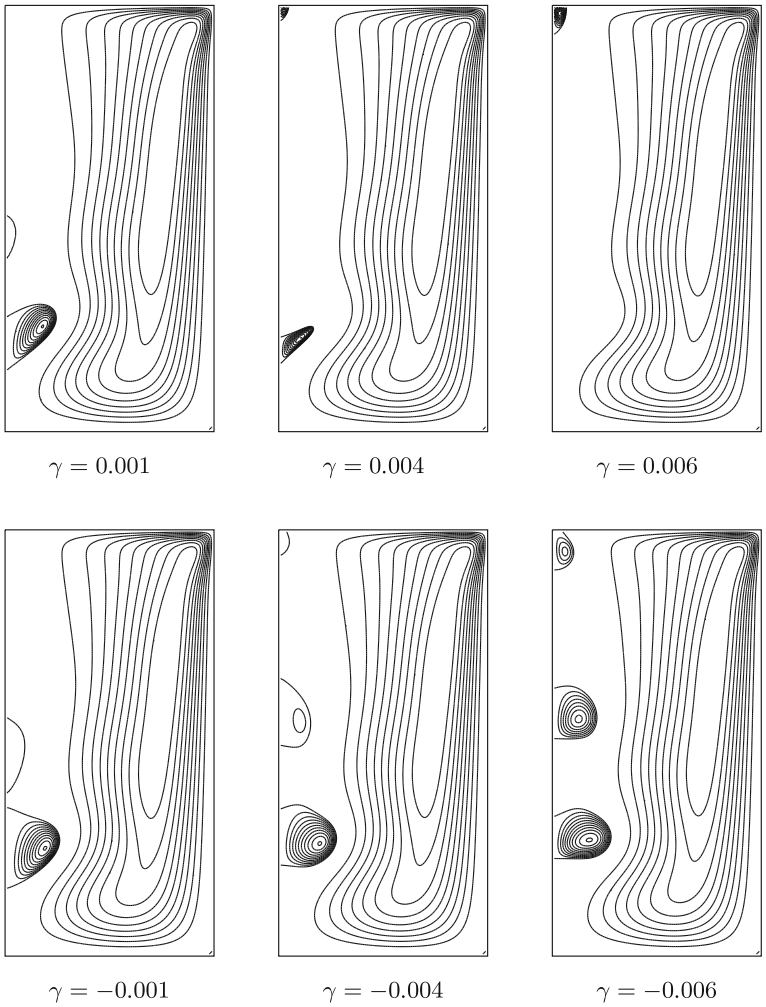


**Fig. 4** Effect of co-rotation (*top row*) and counter-rotation (*bottom row*) of the rod on the flow for $Re_{\text{lid}} = 2200$ and various values of $\gamma$

where $\rho$ is the axial distance over which the velocity jump takes place. As this vorticity source is always negative it induces an axial velocity in the same direction as the bulk flow. Figure 4, however, does not show any vortex near the fixed lid. The reason is that the vorticity source has the same sign as the local vorticity of the bulk flow, and its strength is too small to be visible in a streamline plot. However, by inspection of an iso-vorticity plot (not shown), it is clear that a local accumulation of vorticity can be detected in that location, i.e., near the corner between the rod and the fixed lid. These features of the flow have been sketched in Fig. 6.

### 4.4 Effect of introducing local vorticity sources in the numerical simulation

In order to check the effect of introducing vorticity sources, numerical simulations were carried out for the basic configuration of the flow in a cavity (without rod), in which vorticity sources were implemented by adding a source term $\phi/\Delta z$, to the right-hand side of the vorticity transport equation (Eq. 8). The axial length scale $\Delta z$ was set to the axial grid cell size, which makes the influence of the added source term independent of the grid size.

In the numerical scheme, we let $\phi = 0$, except in the nine grid cells centered around the single grid point of the desired vorticity source. The contribution of the vorticity sources in the nine grid cells were weighted by 1/4 in the center, 1/8 on the sides, and 1/16 in the corners. From the simulations, it was found that a positive vorticity source near the rotating lid causes larger and stronger breakdown bubbles, while a negative vorticity


**Fig. 5** Simulated visualization of the transient flow at $Re_{\text{lid}} = 2200$ for a suddenly started rotation of an initially fixed rod with $\gamma = 0.008$, showing that the breakdown bubbles move up and dissipate in the boundary layer of the lid

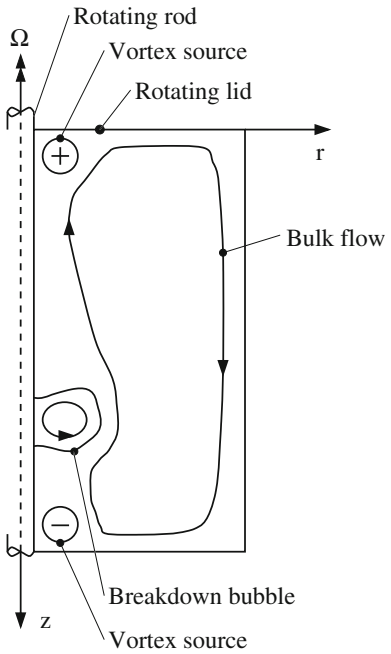


**Fig. 6** Sketch of the flow in the computational domain. The vorticity sources generated by the rotation of the rod are indicated near the top and near the fixed lid of the cavity

source near the rotating lid was observed to weaken and eventually remove the bubbles. Likewise, a negative vorticity source near the fixed lid removes the breakdown bubbles, while a positive vorticity source near the fixed lid strengthens the breakdown bubbles, although the latter case does not correspond to the case with the rotating rod along the center axis. Examples of computations illustrating these phenomena are shown in Fig. 7. Figure 7a shows that a negative vorticity source term introduced near the fixed lid causes the breakdown

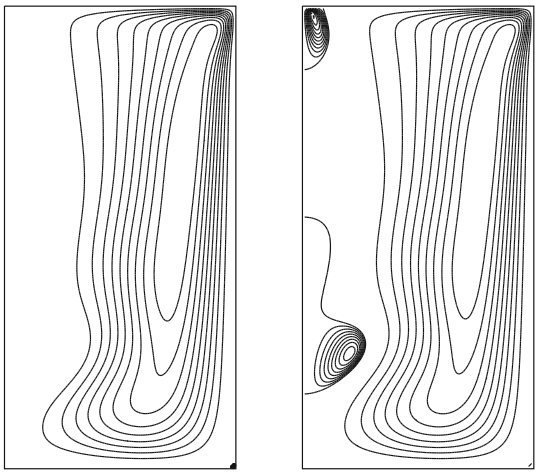


**Fig. 7** Flow in the cavity at $Re_{\text{lid}} = 2200$ controlled by one vorticity source. **a** The breakdown bubbles disappear when a negative vorticity source term is introduced at a location near the fixed lid of the cavity. The applied source term is such that $\phi(1.98, 0.0392) = -6.0$. No actual vortex is visible as the added vorticity blends with the rest of the vorticity field. **b** The breakdown bubbles increase in size and merge when a positive vorticity source term is introduced at a location near the rotating lid. The applied source term is such that $\phi(0.02, 0.0392) = 5.0$. This causes the formation of a vortex in the corner between the center axis and the rotating lid

bubbles to disappear. No additional vortex is created by the source term as the generated vorticity blends with the rest of the vorticity field. In contrast, Fig. 7b shows that a positive vorticity source term introduced near the rotating lid makes the breakdown bubbles increase in size and merge. In this case, a vortex generated by the source term appears in the corner between the center axis and the rotating lid.

Our numerical simulations further indicate that when both sources are present, it is the balance between the positive vorticity source near the rotating lid and the negative vorticity source near the fixed lid that controls the vortex breakdown. This balance is affected by the strength and position of each vorticity source. Numerical simulations demonstrate that the effect of a vorticity source located very close to the rotating lid is weaker than that of a similar vorticity source positioned further away from the rotating lid. Likewise, a vorticity source has a weaker effect when it is placed very close to the fixed lid.

Figure 8 displays results from simulations performed with two vorticity sources. In Fig. 8a, the vorticity source term near the fixed lid dominates the flow, thereby causing the breakdown bubbles to disappear. The streamline patterns resemble those of the flow with a co-rotating rod. In Fig. 8b, the vorticity source term near the rotating lid dominates the flow and the breakdown bubbles are observed to increase in size. This situation is similar to that observed for the flow with a counter-rotating rod. Thus, it is possible to synthesize a vorticity source field, with only two point sources, which has the same effect on the flow as the actual source field produced in the flow with a rotating rod.

## 5 Discussions

While it is clear from the previous analyses and simulations that the presence of corner vorticity sources (either close to the rotating lid or the fixed bottom) can dramatically affect the breakdown bubbles (either significantly diminishing, until they fully disappear, or amplifying them), we now wish to understand the connection between such vorticity sources and the axial velocity. To this end, we use the induction law of Biot–Savart to derive the induced axial velocity from a circular vorticity source placed close to the fixed wall. For the sake of simplicity, we limit the analysis to the center axis. For this, we suppose that the flow is inviscid and curl free, except for the vorticity source. In order to satisfy the no-slip conditions on the fixed wall, we introduce a mirror vorticity source on the opposite side of the wall as shown in Fig. 10. This does not satisfy the boundary conditions on the cylinder wall and on the rotating lid. However, the induction is mainly felt locally, and, as will be discussed later, decreases fast with increasing distance from the sources. For this derivation, we let the $z$-axis originate at the center of the fixed lid and point toward the rotating lid. This is opposite to the orientation of the $z$-axis utilized in the numerical simulations. Note that this implies that a negative vorticity source in the numerical model corresponds to a positive vorcitity source in the analytical model.

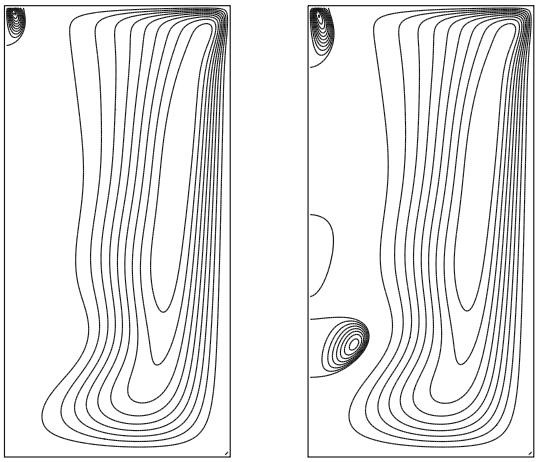

**(a)** **(b)**

**Fig. 8** Flow in the cavity at $Re_{\text{lid}} = 2200$ controlled by two vorticity sources. **a** Flow with vorticity source $\phi(0.01, 0.0392) = 10.0$ at the top of the cavity and vorticity source $\phi(1.98, 0.0392) = -6.0$ at the fixed lid of the cavity. The breakdown bubbles disappear. **b** Flow with vorticity source $\phi(0.02, 0.0392) = 5.0$ at the top of the cavity and vorticity source $\phi(1.99, 0.0392) = -6.0$ at the fixed lid of the cavity. The breakdown bubbles increase in size

First, let us consider a single circular vorticity source with radius $a$ such as the one shown in Fig. 9. Also, let the distance from the center of the circle to the induction point be $z_s$. The vector from a point on the circle toward the point of induction is called $\boldsymbol{R}$. As the problem is axisymmetric, we consider the meridional plane to be aligned with this vector. The Biot–Savart law of induction then gives us

$$\boldsymbol{U} = -\frac{1}{4\pi}\int_V \frac{\boldsymbol{R}\times\boldsymbol{\omega}}{R^3}\mathrm{d}V. \tag{10}$$

Since $\boldsymbol{\omega}$ is orthogonal to $\boldsymbol{R}$, the cross product is aligned with the unit vector in the meridional plane,

$$\left(-\frac{z_s}{R}, 0, -\frac{a}{R}\right),$$

which is orthogonal to $\boldsymbol{R}$. The axial component of this unit vector is $-a/R$. Integrating over the circular ring with cross section $\Delta\alpha$, we calculate the induced axial velocity on the center axis as

$$U_z = -\frac{1}{4\pi}\int_0^{2\pi} \frac{R\omega}{R^3}\left(-\frac{a}{R}\right) a\,\Delta\alpha\,\mathrm{d}\phi, \tag{11}$$

where $R^2 = z_s^2 + a^2$. Hence,

$$U_z = \frac{1}{4\pi}\frac{\Gamma}{R^3}2\pi a^2, \tag{12}$$

where $\Gamma = \omega\,\Delta\alpha$ is the circulation. Thus, we find

$$U_z = \frac{\Gamma a^2}{2\left(z_s^2 + a^2\right)^{\frac{3}{2}}}. \tag{13}$$

Now, wishing to satisfy the boundary conditions on the fixed wall, we return to the problem of two concentric circular vorticity sources as shown in Fig. 10. Let $z_p$ denote the distance from the wall to the point of induction. Evaluating Eq. 10 with the induction from the two circular vorticity sources, each separated by a distance $c$ from the wall, results in the following expression for the induced axial velocity

$$U_z = -\frac{1}{4\pi}\int_0^{2\pi}\left(\frac{R_u\omega}{R_u^3}\left(-\frac{a}{R_u}\right) + \frac{R_d(-\omega)}{R_d^3}\left(-\frac{a}{R_d}\right)\right) a\,\Delta\alpha\,\mathrm{d}\phi, \tag{14}$$

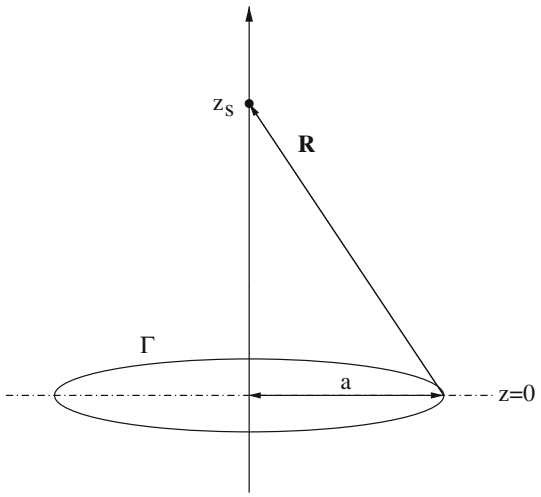


**Fig. 9** Sketch of a ring-shaped vorticity source with circulation Γ. Also shown is the vector from a point on the circumference of the vorticity source towards the induction point $z_s$ on the center axis

where the subscripts u and d denote the upper and lower vorticity source, respectively. Note the opposite signs of vorticity for the two circular rings. This yields

$$U_z = \frac{\Gamma a^2}{2}\left[\frac{1}{\left((z_p - c)^2 + a^2\right)^{\frac{3}{2}}} - \frac{1}{\left((z_p + c)^2 + a^2\right)^{\frac{3}{2}}}\right]. \tag{15}$$

Requiring that $c << z_p$, this expression can be approximated via a Taylor series by

$$U_z = \frac{3\Gamma a^2 c z_p}{\left(z_p^2 + a^2\right)^{\frac{5}{2}}}. \tag{16}$$

Here, the other effects such as those due to the presence of boundary layers and convective effects are not included in our analysis.

The additional velocity induced by the vorticity source is the difference between the velocity of the flow computed with the vorticity source and the velocity of the basic flow configuration without the vorticity source (and without rod). In this study, the simulations were carried out for the Reynolds number $Re_{\mathrm{lid}} = 2200$. Figure 11 shows that there is indeed a good agreement between this axial velocity difference and the induced velocity given by Eq. 15, although, the analytical solution gives systematically lower values than the numerical velocity difference. The slower decrease of the numerically modeled velocity difference compared to the induced velocity of the analytical model is likely due to the influence of the nonlinear convection that tends to redistribute the vorticity.

We now recall that vortex breakdown in the closed cavity is a separation phenomenon with a reverse flow taking place within the separation bubbles. Given this reverse flow, the question is whether the vorticity source is capable of generating a sufficiently strong induced axial velocity to overcome the reverse flow inside the bubbles, and therefore suppress the bubbles altogether. Indeed, the absolute axial velocity of the reverse flow through both breakdown bubbles is found to be smaller than the induced velocity, whether the latter is deduced either from the analytical model or from the numerical simulations. Thus, the analytical model can be utilized to explain the disappearance of the breakdown bubbles in the cavity flow with a vorticity source near the fixed wall. Since the vorticity source is similar to the vorticity generated in the flow with a rotating rod, we have hereby found an analytical model capable of explaining the underlying control mechanism of the rod as well.

However, we have also observed, in the numerical simulations, that the occurrence of the breakdown bubbles in the controlled flow is highly sensitive to the position of the vorticity source within the boundary layer near the fixed wall. The part of this dependence due to linear effects can be accounted for by Eq. 16. Away

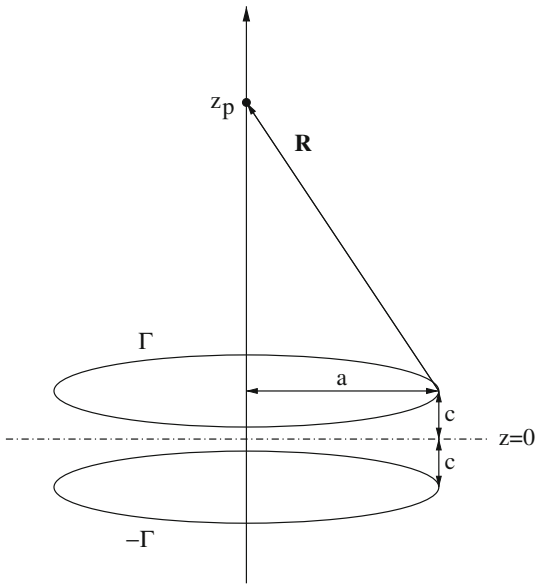


**Fig. 10** Sketch of a ring-shaped vorticity source with circulation $\Gamma$ placed at a distance $c$ above the fixed wall of the cavity together with its mirror image with circulation $-\Gamma$. Also shown is the vector from a point on the circumference of the upper vorticity source toward the induction point $z_p$ on the center axis

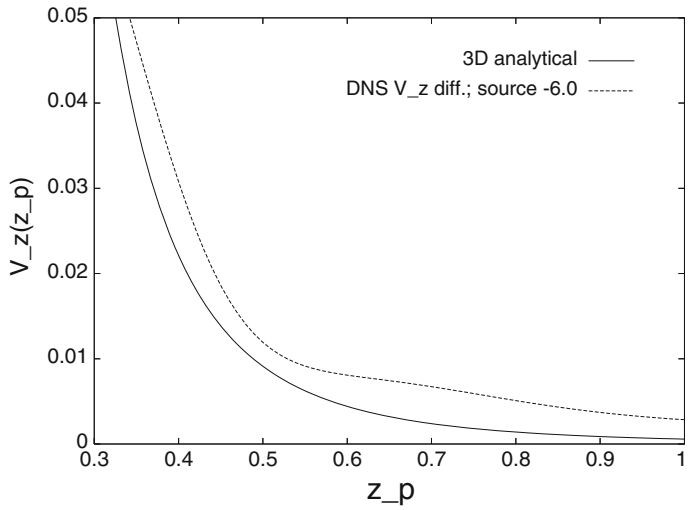


**Fig. 11** Axial velocity at a point along the cylinder axis induced by a vorticity source (see Fig. 10) as a function of the distance from the wall. The analytical model of induced axial velocity is compared with the difference between the numerically simulated velocity of the flow with the vorticity source near the fixed wall and that of the flow without vorticity source. A good agreement between the curves is seen. The Reynolds number is $Re_{\mathrm{lid}} = 2200$. The *full line* represents the induced velocity of the analytical model. The *dashed line* represents the axial velocity difference of the numerical simulations

from the fixed wall, assuming $z_p >> a$, we obtain

$$U_z = \frac{3\Gamma a^2 c}{z_p^4}. \tag{17}$$

This expression shows that the induced axial velocity behaves like $a^2$ and $c$ in the radial and axial directions, respectively. The dependence in the axial direction was found to be more sensitive in the numerical simulations than predicted by Eq. 17 due to the influence of the boundary layer. In addition, the axial velocity behaves as $z_p^{-4}$ according to the above equation.

A similar analytical model can be used to explain the behavior observed in the experimental study of Mununga et al. [15], in which a small counter-rotating disk placed in the center of the end-wall opposite to the driving lid was found to suppress breakdown bubbles. As there is no rod, an argument based on the reduction of the adverse pressure gradient along the axis due to a $z$-independent swirl, generated by the rod, does not apply. However, utilizing the coordinate system of the numerical model, the source term of Eq. 9 becomes negative in the vicinity of the small disk due to the negative gradient of $v_\theta^2$ outside the layer of zero $v_\theta$ near the disk. Although, in this case, there is also a positive vorticity source located closer to the small disk, it is likely that the influence of the negative vorticity source dominates, as the source is located further away from the wall. Thus, counter-rotation results in suppressing breakdown bubbles in this situation. In the case of co-rotation, a positive vorticity source generated near the small disk enhances the breakdown bubbles, as predicted by our simulations and the arguments used in this article.

## 6 Conclusions

Vortex breakdown within a closed cylinder with a rotating lid has been controlled successfully in numerical simulations for varying parameter values by the introduction of a thin rotating rod along the center axis. Breakdown bubbles are either prevented by co-rotation or promoted by counter-rotation of the rod. Although this is a known result from previous experimental study [10], to the best of our knowledge, it is shown for the first time numerically. Furthermore, our simulations revealed that rotating the rod results in the local generation of negative vorticity near the fixed lid and positive vorticity near the rotating lid. It follows that the prevention of vortex breakdown can also be achieved by adding negative vorticity close to the center axis near the fixed lid of a cavity flow, which induces an axial velocity in the same direction as the bulk flow. Likewise, the promotion of vortex breakdown can be obtained by adding positive vorticity close to the center axis near the rotating lid, which induces an axial velocity against the direction of the bulk flow. It was demonstrated that the competition between these two mechanisms controls the streamline topology when the rod rotates. We have also described the influence of a vorticity source by an analytical model of the induced axial velocity, which corresponds to the additional axial velocity induced by the vorticity field generated by a counter-rotating rod. The induced axial velocity was found to be sufficient to overcome the reverse flow inside the breakdown bubbles and therefore suppresses the bubbles. Hence, we have presented an analytical model explaining the underlying control mechanism of the rotating rod. Finally, these results imply that such a suppression and enhancement of vortex breakdown based on the addition of negative and positive vorticity sources in the flow can be achieved by other types of control devices, such as a small rotating disk or possibly small particles, which can be put into rotation by an external electric (or magnetic) field in a microfluidic device. This might also be a step in the direction of understanding and controlling vortex breakdown in other, perhaps more complicated, flow geometries.

**Acknowledgments** We would like to thank M. O. L. Hansen for providing numerical verification of our analytical model. Also, we would like to thank V. Okulov for providing useful suggestions about presenting our analysis. One of us, B. H. Jørgensen, would like to thank Professor P. Videbech, for helpful advice.

## References

1. Blackburn, H.M., Lopez, L.M.: Modulated rotating waves in an enclosed swirling flow. J. Fluid Mech. **465**, 33–58 (2002)
2. Brown, G.L., Lopez, J.M.: Axisymmetric vortex breakdown part 2. Physical mechanisms. J. Fluid Mech. **221**, 553–576 (1990)
3. Buchhave, P., Jakobsen, M.L., Westergaard, C.H., Sørensen, J.N.: PIV: measurement of the early transition of a rotating flow in a closed cylinder. Fourth International Conference on Laser Anemometry, Advances and Applications, Cleveland, Ohio (1991)
4. Daube, O., Sørensen, J.N.: Simulation numérique de l'ecoulement periodique axisymmetrique dans une cavité cylindrique. C. R. Acad. Sci. Paris **308**(2), 463–469 (1989)
5. Daube, O., Loc, T.P., Monet, P., Coutanceau, M.: Ecoulement instationaire décollé d'un fluide incompressible autour d'un profil: une comparaison theorié-experience. Technical Report CP 366, AGARD (1985)
6. Escudier, M.P.: Observations of the flow produced in a cylindrical container by a rotating endwall. Exp. Fluids **2**, 189–196 (1984)
7. Gelfgat, A.Y., Bar-Yoseph, P.Z., Solan, A.: Three-dimensional instability of axisymmetric flow in rotating lid-cylinder enclosure. J. Fluid Mech. **438**, 363–377 (2001)
8. Herrada, M., Shtern, V.: Vortex breakdown control by adding near-axis swirl and temperature gradients. Phys. Rev. E **68**(041202), 8 (2003)

9. Husain, H., Shtern, V., Hussain, F.: Control of vortex breakdown using vortex generators. 28th AIAA Fluid Dynamics Conference, 4th AIAA Shear Flow Control Conference, Snowmass Village (1997)
10. Husain, H., Shtern, V., Hussain, F.: Control of vortex breakdown by addition of near-axis swirl. Phys. Fluids **15**(2), 271–279 (2003)
11. Lopez, J.M.: Axisymmetric vortex breakdown Part 1. Confined swirling flow. J. Fluid Mech. **221**, 533–552 (1990)
12. Lugt, H.J., Abboud, M.: Axisymmetric vortex breakdown with and without temperature effects in a container with a rotating lid. J. Fluid Mech. **179**, 179–200 (1987)
13. Mullin, T., Tavener, S.J., Cliffe, K.A.: On the creation of stagnation points in a rotating flow. ASME J. Fluids Eng. **120**, 685–689 (1998)
14. Mullin, T., Kobine, J.J., Tavener, S.J., Cliffe, K.A.: On the creation of stagnation points near straight and sloped walls. Phys. Fluids **12**(2), 425–431 (2000)
15. Mununga, L., Hourigan, K., Thompson, M.C., Leweke, T.: Confined flow vortex breakdown control using a small rotating disk. Phys. Fluids **16**(12), 4750–4753 (2004)
16. Pereira, J.C.F., Sousa, J.M.M.: Confined vortex breakdown generated by a rotating cone. J. Fluid Mech. **385**, 287–323 (1999)
17. Ronnenberg, B.: Ein selbstjustierendes 3-komponenten-lda nach dem vergleighstrahlverfaren, angewendt für untersuchungen in einer stationaren zylindersymmetrischen drehströmung mit einem rühckströmgebiet. Technical Report Bericht 20, Max-Planck-Institut für Strömungsforschung, Göttingen (1977)
18. Serre, E., Bontoux, P.: Vortex breakdown in a three-dimensional swirling flow. J. Fluid Mech. **459**, 347–370 (2002)
19. Serre, E., Bontoux, P.: Vortex breakdown in a cylinder with a rotating bottom and a flat stress-free surface. Int. J. Heat Fluid Flow **28**, 229–248 (2007)
20. Sørensen, J.N., Christensen, E.A.: Direct numerical simulation of rotating fluid flow in a closed cylinder. Phys. Fluids **7**(4), 764–778 (1995)
21. Sørensen, J.N., Loc, T.P.: High-order axisymmetric navier-stokes code: description and evaluation of boundary conditions. Int. J. Num. Methods Fluids **9**, 1517 (1989)
22. Sørensen, J.N., Naumov, I., Mikkelsen, R.: Experimental investigation of three-dimensional flow instabilities in a rotating lid-driven cavity. Exp. Fluids **41**, 425–440 (2006)
23. Sotiropoulos, F., Ventikos, Y.: Transition from bubble-type vortex breakdown to columnar vortex in a confined swirling flow. Int. J. Heat Fluid Flow **19**, 446–458 (1998)
24. Sotiropoulos, F., Ventikos, Y.: The three-dimensional structure of confined swirling flows with vortex breakdown. J. Fluid Mech. **426**, 155–175 (2001)
25. Sotiropoulos, F., Ventikos, Y., Lackey, T.C.: Chaotic advection in three-dimensional stationary vortex-breakdown bubbles: Silnikovs chaos and the devils staircase. J. Fluid Mech. **444**, 257–297 (2001)
26. Sotiropoulos, F., Webster, D.R., Lackey, T.C.: Experiments on lagrangian transport in steady vortex-breakdown bubbles in a confined swirling flow. J. Fluid Mech. **466**, 215–248 (2002)
27. Tang, S., Aubry, N.: On the symmetry breaking instability leading to vortex shedding. Phys. Fluids **9**(9), 2550–2561 (1997)
28. Tang, S., Aubry, N.: On the suppression and alteration of vortex shedding. J. Fluids Struct. **14**(3), 443–468 (2000)
29. Vogel, H.U.: Experimentelle ergebnisse über die laminare strömung in einem zylindrischen gehaüse mit darin rotierender scheibe. Technical Report Bericht 6, Max-Planck-Institut für Strömungsforschung, Göttingen (1968)